




The impact of xylem geometry on olive cultivar resistance to *Xylella fastidiosa*: An image-based study

Nancy C. Walker¹ | Steven M. White²  | Dan McKay Fletcher¹ | Siul A. Ruiz¹ | Kathryn E. Rankin^{1,3}  | Angelo De Stradis⁴ | Maria Saponari⁴ | Katherine A. Williams^{1,5} | Chiara Petroselli^{1,6} | Tiina Roose¹ 

¹Bioengineering Sciences Research Group, Department of Mechanical Engineering, School of Engineering, Faculty of Engineering and Physical Sciences, University of Southampton, Southampton, UK

²UK Centre for Ecology & Hydrology, Wallingford, UK

³ μ -VIS X-ray Imaging Centre, Faculty of Engineering and Physical Sciences, University of Southampton, Southampton, UK

⁴Istituto per la Protezione Sostenibile delle Piante, CNR, Bari, Italy

⁵Faculty of Science and Health, University of Portsmouth, Portsmouth, UK

⁶Dipartimento di Chimica, Biologia e Biotecnologie, Università degli Studi di Perugia, Perugia, Italy

Correspondence

Tiina Roose, Bioengineering Sciences Research Group, Department of Mechanical Engineering, School of Engineering, Faculty of Engineering and Physical Sciences, University of Southampton, University Road, Southampton SO17 1BJ, UK.
Email: t.roose@soton.ac.uk

Funding information

Horizon 2020 Framework Programme, Grant/Award Number: 727987-XF-ACTORS, ERC-646809 and 635646-POnTE; Natural Environment Research Council, Grant/Award Number: NE/S00720/1

Abstract

Xylella fastidiosa is a xylem-limited plant pathogen infecting many crops globally and is the cause of the recent olive disease epidemic in Italy. One strategy proposed to mitigate losses is to replant susceptible crops with resistant varieties. Several genetic, biochemical and biophysical traits are associated to *X. fastidiosa* disease resistance. However, mechanisms underpinning resistance are poorly understood. We hypothesize that the susceptibility of olive cultivars to infection will correlate to xylem vessel diameters, with narrower vessels being resistant to air embolisms and having slower flow rates limiting pathogen spread. To test this, we scanned stems from four olive cultivars of varying susceptibility to *X. fastidiosa* using X-ray computed tomography. Scans were processed by a bespoke methodology that segmented vessels, facilitating diameter measurements. Though significant differences were not found comparing stem-average vessel section diameters among cultivars, they were found when comparing diameter distributions. Moreover, the measurements indicated that although vessel diameter distributions may play a role regarding the resistance of Leccino, it is unlikely they do for FS17. Considering Young–Laplace and Hagen–Poiseuille equations, we inferred differences in embolism susceptibility and hydraulic conductivity of the vasculature. Our results suggest susceptible cultivars, having a greater proportion of larger vessels, are more vulnerable to air embolisms. In addition, results suggest that under certain pressure conditions, functional vasculature in susceptible cultivars could be subject to greater stresses than in resistant cultivars. These results support investigation into xylem morphological screening to help inform olive replanting. Furthermore, our framework could test the relevance of xylem geometry to disease resistance in other crops.

KEYWORDS

olive dieback, X-ray computed tomography, *Xylella*

This is an open access article under the terms of the [Creative Commons Attribution](https://creativecommons.org/licenses/by/4.0/) License, which permits use, distribution and reproduction in any medium, provided the original work is properly cited.

© 2022 The Authors. *Plant Pathology* published by John Wiley & Sons Ltd on behalf of British Society for Plant Pathology.

1 | INTRODUCTION

Xylella fastidiosa (Wells et al., 1987) is a plant-pathogenic bacterium that colonizes xylem vessels, that is, vasculature that transports water, and is spread from host to host by xylem-feeding insects. The potential host pool comprises more than 500 plant species. In some hosts *X. fastidiosa* is a harmless endophyte, whilst in others it causes severe disease (Delbianco et al., 2022). Importantly, *X. fastidiosa* is the cause of a number of diseases in crops of high economic importance, such as grapevine, coffee and citrus. In particular, a recent introduction of *X. fastidiosa* subsp. *pauca* sequence type ST53 (the specific strain causing the olive quick decline syndrome in the region) in Puglia, Italy, has resulted in a novel olive disease outbreak: the olive quick decline syndrome (Saponari et al., 2013).

Symptoms caused by *X. fastidiosa* infection are nonspecific and are mostly similar to those of water stress. Early symptoms include leaf scorch and wilt, which later progress to severe dieback and whole plant death. Signs of disease appear to be caused by both the production of biofilm by the bacterium and structures formed in the plant defence response, both of which impede sap flow (Roper et al., 2019). In particular, it has been shown that the occlusion of petiole vessels, those in the stalks that attach leaves to stems, by these structures has a primary role in *X. fastidiosa* pathogenicity (Cardinale et al., 2018). Within an infected host, localized colonies of *X. fastidiosa* cells aggregate in xylem vessels, directly blocking sap ascent. This observed aggregation corresponds to the development of biofilms, a heterogeneous microbial community attached to the xylem vessel wall. In a biofilm, cells are bound to each other and to the wall by a self-produced matrix of extracellular polymeric substances that are key to the biofilm's physical integrity (Vert et al., 2012). As well as the impedance to healthy xylem flow resulting directly from the presence of *X. fastidiosa* biofilms, excessive and ineffective plant immune responses produce additional vessel blockages. A common physical defence mechanism in xylem vessels is the formation of tyloses, which are bubble-like structures formed by living cells surrounding the vessel. They are produced when such a cell pushes into the centre of the vessel via one of many small perforations in the vessel wall, known as vessel pits. Once bridging the entire vessel diameter, these structures are able to compartmentalize a section of the vessel. Though there is limited evidence, it is thought that this compartmentalization acts to prevent the spread of pathogens through the plant or, as often in the case of drought, to seal off vessels embolized by air bubbles that are no longer functional (De Micco et al., 2016). Importantly, the overproduction of tyloses in response to biotic stress can cause a detrimental reduction in hydraulic conductivity within the xylem (Collins et al., 2009; McElrone et al., 2010). In addition, evidence suggests that the timing of tylose production can have critical consequences for a plant's response to infection (De Benedictis et al., 2017). In particular, if tylose production is delayed under infection, the pathogen can become systemic in the plant before they are produced. If the immune response is delayed in this way, tyloses only restrict sap flow, worsening disease symptoms (Sun et al., 2013).

Currently there is no proven cure for *X. fastidiosa*-infected plants under field conditions (Bragard et al., 2019). However, it has been found that in known susceptible taxa, such as grapevines and olives where the pathogen causes distinctive outbreaks, there can be significant variations in symptom expression and transmissibility between genetically and phenotypically different hosts (Sabella et al., 2019). Whilst some hosts are susceptible, with high pathogen populations in all tissues and severe symptoms, others exhibit tolerance. Although bacterial counts remain high in tolerant hosts, impact on their health is reduced. Some hosts, termed resistant, exhibit both low bacterial counts and limited symptom expression (Agrios, 2005). Current opinion suggests that, where possible, replanting with plant varieties that are resistant to disease presents the most promising strategy in an attempt to adapt to *X. fastidiosa* in affected regions (Pavan et al., 2021; Saponari, Altamura, et al., 2019).

In the Mediterranean basin, cultivated olive species have large (>900 cultivars) genetic and phenotypic variability (Muzzalupo et al., 2009) within which resistance has already been demonstrated. As soon as the epidemic started spreading in Puglia, several field observations indicated that, whilst the widely represented traditional cultivars Ogliarola Salentina and Cellina di Nardò were highly susceptible to *X. fastidiosa*, other less abundant cultivars showed mild disease symptoms typical of resistant and tolerant plants (Saponari, Giampetruzzi, et al., 2019). This prompted the start of large-scale field trials considering several different cultivars in the infected area so that their response to infection could be monitored (Saponari, Giampetruzzi, et al., 2019). It was observed that trees of cultivar Leccino were symptomless or showed very mild dieback, despite being adjacent to trees showing very severe symptoms (Saponari, Giampetruzzi, et al., 2019). The resistance of Leccino has since been confirmed by several research teams and field-based studies, showing Leccino harbours lower bacterial loads in comparison to other susceptible cultivars (Boscia et al., 2017; Giampetruzzi et al., 2016; Luvisi et al., 2017; Saponari et al., 2017). Resistance has also been confirmed in FS17 (also known as Favolosa), a more recent cultivar found to express even lower bacterial loads than Leccino (Boscia et al., 2017). As a result of amendment to legislation (European Union, 2017), both Leccino and FS17 may now be replanted in the infected zone. Some *X. fastidiosa*-resistant varieties of other plant host species have similarly been identified (Coletta-Filho et al., 2007; Krivanek & Walker, 2005) and a number of other olive cultivars are currently under evaluation regarding their susceptibility to infection (Saponari, Altamura, et al., 2019). However, mechanisms underpinning resistance are still poorly characterized. Understanding these mechanisms is currently one of the primary focuses of the research community.

Some work has been done on investigating mechanisms underlying the *X. fastidiosa* disease resistance of Leccino. Studies have found differences both in the cultivar's genetics (De Pascali et al., 2019, 2022; Giampetruzzi et al., 2016) and in its xylem ionic and biochemical properties (D'Attoma et al., 2019; Giampetruzzi et al., 2016; Sabella et al., 2018) that may contribute to its resistance. For example, the presence of lignin has been associated with the resistance of



Leccino (Sabella et al., 2018). Lignin is a molecule known to reinforce vasculature cells, which might provide structural support for vessels and make it more difficult for the bacteria to pass between adjacent vessels. Plant hormone signalling also appears to have a role in resistance, as certain signals are often associated with biotrophic and necrotrophic interactions. However, direct relationships between signalling and resistance are often difficult to quantify, as these interactions are complex (Choi et al., 2013).

Xylem anatomy and physiology has also been suggested to play a role in disease resistance. Chatelet et al. (2011) showed that *X. fastidiosa*-resistant grapevines have on average smaller diameter vessels than susceptible ones. Similarly, studies suggest xylem vessel diameters probably play a role in the resistance of olive cultivar Leccino (Petit et al., 2021; Sabella et al., 2019). In particular, smaller diameter vessels are reported in Leccino in comparison with plants of susceptible cultivar Cellina di Nardò (Petit et al., 2021; Sabella et al., 2019). Moreover, Sabella et al. (2019) made some general hypotheses as to how narrow vessels could be acting as a resistance mechanism in Leccino. In particular, these authors hypothesized that narrower vessels limit pathogen spread in the plant due to a slower flow rate, and that their lower susceptibility to air embolism results in less cavitation and is less favourable for the aerobic metabolism of the bacteria. However, no evidence could be given for these mechanisms, and thus they remain only speculative. Furthermore, investigation into the influence of vessel diameter on olive cultivar resistance has not yet extended beyond cultivars Leccino and Cellina di Nardò. This represents a significant gap in the literature; without consideration of other cultivars, it is impossible to predict the general relevance of narrow vessels as a resistance trait. Not only this, but previous studies have only been able to make a limited number of measurements due to the two-dimensional nature of the imaging technique and lack of postprocessing.

One avenue to bridge some of these existing knowledge gaps is through the use of 3D X-ray computed tomography (CT). X-ray CT is a technique that presents several advantages to traditional thin slicing microscopy for quantitative wood anatomy, including the quantification of xylem vessels (Van den Bulcke et al., 2009). The destructive nature of thin sectioning, which is avoided by using CT, results in limited sampling of anatomical features. In addition, X-ray CT images have the advantage of maintaining consistent alignment across slices. Images are resolved with an isotropic voxel size, which enables the volumes to be reoriented and resliced in any desired plane. This consistency in alignment is difficult to achieve when taking thin sections. Finally, due to the volumetric nature of the data, vessel section diameters can be characterized along their entire lengths, removing the need to do any stereological data conversions.

In the present study, xylem vessel diameters were measured in stems from trees of four different olive cultivars of varying susceptibility to *X. fastidiosa*, namely Koroneiki, Ogliarola, FS17 and Leccino. Vessel diameter measurements were extracted from high-resolution 3D X-ray CT (μ CT) (Landis & Keane, 2010) images via a bespoke methodology, defining diameters on the basis of measurements obtained over entire vessel section lengths. Using the obtained vessel

diameter size distributions, we investigate whether trends in this anatomical trait can be associated to the degree to which the considered olive cultivars are susceptible or resistant to *X. fastidiosa*. In addition, the xylem vessel diameter measurements were used in conjunction with fluid mechanical and hydrological principles to assess differences in embolism susceptibility and cultivar hydraulic conductivity via xylem flow rates.

2 | MATERIALS AND METHODS

2.1 | Choice of cultivars

Samples were taken from young trees (2-year-old self-rooted potted plants) from a nursery in Calabria, Italy. Samples were selected from plants of two cultivars categorized as susceptible (Ogliarola and Koroneiki) and two resistant (Leccino and FS17) to *X. fastidiosa* infection. We chose these four cultivars based on existing molecular and field evidence. Bacterial populations were measured in infected plants by quantitative PCR (qPCR) and symptom scores given on the basis of field observations. Data supporting the categorization of three cultivars can be found in Table S1. Data supporting the resistance of FS17 can be found in the work of Giampetruzzi et al. (2020).

2.2 | Sample selection and preparation

We prepared samples from three replicates of each cultivar for scanning. We cut young branches from each tree, sampling at a point in the stem that was approximately 2 mm thick. Samples of this diameter were chosen to select for approximately 1-year-old semihardwood stems. Both molecular and cytopathological evidence show that *X. fastidiosa* replicates and damages the xylem in vessels of 1-year-old stems (Montilon et al., 2022). The age of the stem is a developmental parameter that makes the comparison between cultivars uniform. In addition, it is reported that for detection, it is important that semihardwood stems are examined (D'Onghia et al., 2021). In general, semihardwood stems are those of maximum 5 mm in diameter (D'Onghia et al., 2021). It was important to select semihardwood stems due to their importance in infection development.

After the samples were trimmed, they were dried under controlled conditions for a week in a Conviron CMP6010 growth chamber (Controlled Environments Ltd). This was to limit motion artefacts due to shrinkage driven by moisture loss that would otherwise occur during scanning. We also note that a very high moisture content could impact the contrast to noise ratio, as water is highly absorbent of X-rays. By applying this drying process, we assume that shrinking of vessel pores due to moisture loss during drying is uniform across vessels, that is, all vessels from all stems will be affected in a linear manner. As such, comparisons between the measurements will remain representative. The growth chamber was set at 22°C and lowest possible (set to zero) humidity. The dried samples were then cut down further using a sharp blade to approximately 5–10 mm in

length. To limit motion artefacts from lateral movement, samples were surrounded by a thin layer of foam placed inside 3 mm inner-diameter/4 mm outer-diameter carbon fibre tubing held in a custom 3D printed mount. We note that one of the Koroneiki replicates was much larger in diameter than all of the other samples. As such we did not include this sample in our analyses. The elimination of this replicate as an outlier is described in [Text S1](#).

2.3 | X-ray CT scanning and image processing

All μ CT data was acquired using the Zeiss Xradia Versa 510 X-ray microscope CT scanner (Carl Zeiss) at the μ -VIS Centre for Computed Tomography at the University of Southampton. This scanner operates by a two-stage magnification. Primary magnification is geometric, determined by the X-ray cone beam and source-to-object and source-to-detector distances. Secondary magnification occurs post-scintillation as optical microscope objective lenses further magnify the image ahead of a charged-coupled device (CCD) detector. For each sample, projection data were acquired using an energy of 80 kVp and a power of 7 W. Source to object and source to detector distances were 11 mm and 37 mm, respectively. We used a 2026 \times 2026 pixels CCD detector with 1 \times binning, together with a 4 \times objective lens. A total of 4001 projections were collected over 360 $^\circ$ rotation. The exposure time of each projection was 4 s, and the average scan time for each sample was 5 h 38 min. Following the acquisition, the raw data were reconstructed using XM Reconstructor software (Carl Zeiss), which used a filtered back projection algorithm producing a 16-bit raw volume. Individual elements of reconstructed CT data are called voxels, three-dimensional pixels. The grey value of a voxel is governed by the X-ray absorbance at the spatial location that the voxel represents, which correlates with density of the material. The resolution of our images, given by the voxel side length, is 1 μ m.

Xylem vessels were located in the images (segmented) and analysed using the developed custom workflow illustrated in [Figure 1](#). The workflow was implemented in the FIJI distribution of ImageJ (Rueden et al., 2017; Schindelin et al., 2012), an open-source software package for image processing and analysis, and Python 3 (Van Rossum & Drake, 2009). All processes were carried out on specialist high-memory computers (256 GB RAM) in the μ -VIS Centre IT Suite.

Our raw data were reduced to 8-bit depth while maintaining a dynamic range and exported as a tiff-stack. An 8-bit depth was chosen to reduce memory requirements and computational time. Removing the first 100 image slices, the following 1800 slices were selected for processing. The purpose of this was to make the stack sizes uniform, and to remove slices from top and bottom for which the images are often noisy due to the conical shape of the X-ray beam (cone beam artefacts).

The xylem tissue was then segmented from the rest of the image using a manual approach ([Figure 1b](#)). After every 200 slices, the outer boundary of the xylem tissue was selected by manually drawing a polygon (*polygon tool*) around its outer and inner edges. The selection was saved using the ROI (region of interest) manager in FIJI, and a linear

interpolation applied to make an appropriate selection for intermediate image slices. The grey-value of voxels outside of the selected region were set to zero, resulting in an image stack where only the xylem tissue had non-zero grey values (see identified xylem tissue in [Figure 1a](#)).

With the xylem tissue isolated, the xylem vessel pores were segmented using an automated approach ([Figure 1c](#)). The steps required to achieve this are visualized in 2D in [Figure 1d–g](#). The segmentation classified remaining non-zero grey-value voxels into two classes corresponding to tissue and air (pore). To achieve this automated segmentation, the xylem tissue stack was first filtered using a 3D median filter, with a radius of two voxels. For a given voxel in the image, the median filter will take the values of all the neighbouring voxels within the selected radius (two voxels) and determine the median value. That value of the voxel will then be changed to the value of the local median. This is an effective method for filtering out isolated extreme grey value voxels, whilst preserving the relevant data. This removed some noise in the image, helping to separate voxel classes in accordance with the anatomy. After filtering, the image stacks were converted to 32-bit before automatic thresholding using the Otsu thresholding algorithm (Otsu, 1979) ([Figure 1e](#)). When the histogram of voxel grey-values is bimodal, the Otsu method works to separate grey values in the histogram into two distinct classes (in this case tissue and pore), with a threshold defined as a result of minimization of the weighted variance of these classes. The images were converted to 32-bit before applying the Otsu algorithm so that background voxels (already segmented out by the manual segmentation) could be set to NaN so that they are not included in determining the pixel class separation.

Though the Otsu algorithm locates the pore space, corrections were necessary to remove artefacts ([Figure 1f](#)). X-ray CT is particularly sensitive to abrupt changes in the decrement of the refractive index, occurring when the X-rays pass between two materials of highly contrasting densities. This leads to stronger contrast outlining structural boundaries (edge enhancement) compared with a conventional radiogram. This edge enhancement has the effect of creating subtle bright and dark highlights on either side of any edges in the image, called overshoot and undershoot. This meant that, particularly for the larger diameter vessels, the centre was not always included in the threshold, whilst voxels just outside the vessel boundary were sometimes included. To correct for this, ImageJ *fill holes* and *watershed* binary processes were applied to each slice in the stacks. *Fill holes* adds any pixels fully surrounded by already selected pixels into the segmentation. In our images, such pixels corresponded to the vessel centres missed by Otsu. *Watershed* removes the effect of the overshoot artificially connecting vessels. It works by creating a distance map between the centre of every object in the segmentation (which we will call 'candidate vessel sections') and its boundary. Where two of these maps overlap defines the line along which two candidate vessel sections should be separated. To reduce the size of the image files, a bounding box was used to remove unnecessary background before saving the resulting thresholded images. The resulting 'segmented' stack could be saved as a stack of 8-bit tif files, corresponding to the lowest available bit depth.

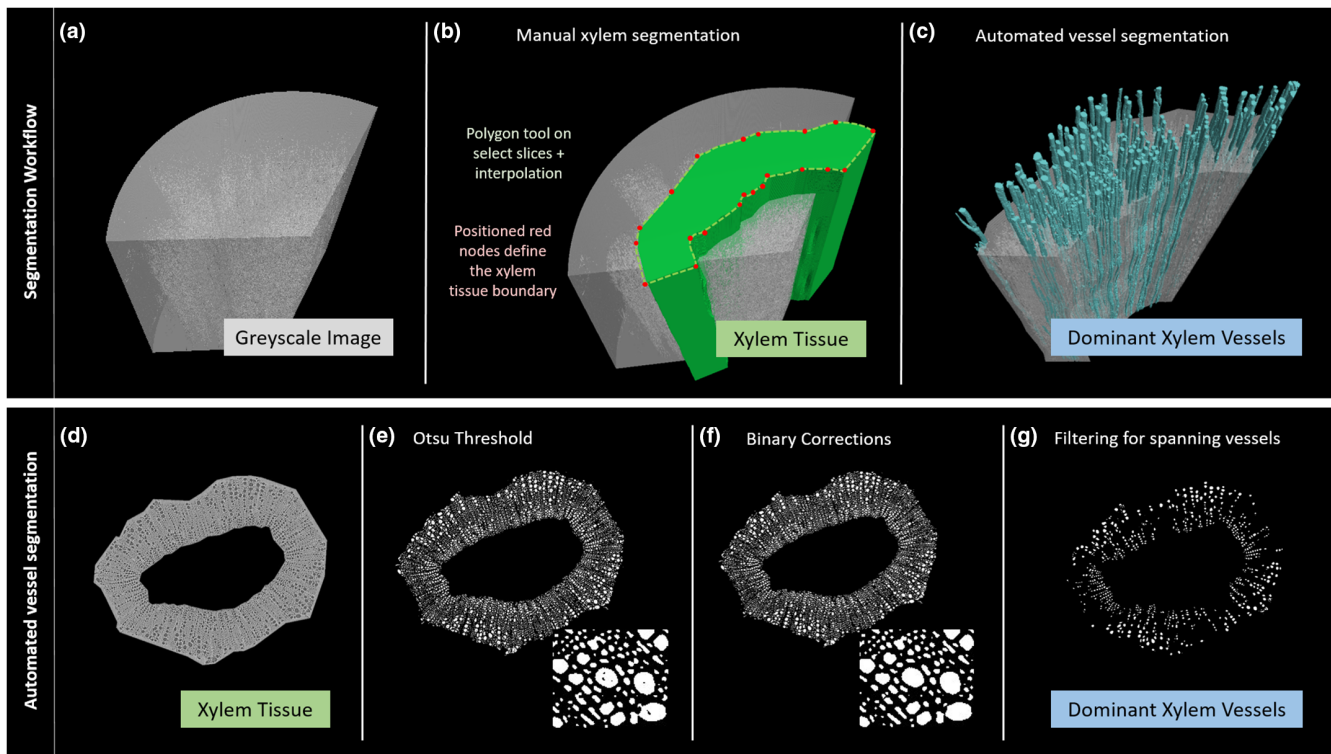


FIGURE 1 Custom image processing workflow—a visual flow chart describing the image processing workflow used for segmenting xylem vessels (a–c). Image processing was completed in the FIJI distribution of ImageJ (Schindelin et al., 2012), and Python3. First, a manual segmentation was applied to isolate the xylem tissue (b). We drew around the tissue using the FIJI polygon tool on a number of image slices, and interpolated between our selected regions to infer the location of the xylem tissue on intermediate slices. Then, an automated segmentation was applied to isolate the considered spanning vessels from the tissue (c). The automated segmentation involved a number of steps, visualized in 2D (d–g). First, an Otsu threshold isolated the pore space (e). Next, a number of simple processes applied to the binary images were used to correct for imaging artefacts (f). Finally, unique vessels were labelled using FIJI simple segmentation, from which spanning vessels were determined in Python3 (g). This was done by checking which labels appeared on both top and bottom scan slices. [Colour figure can be viewed at [wileyonlinelibrary.com](https://onlinelibrary.wiley.com)]

2.4 | Assessment of xylem vessel diameters

We quantified xylem vessel diameters using the segmented image stacks. To first identify the candidate vessel sections, as selected by the segmentation, we made use of plug-ins found in the 3D ImageJ Suite (Ollion et al., 2013). First, we applied a 3D erosion to our segmented stacks to ensure we had disconnected any artificially touching candidate vessel sections. Then we applied a 32-bit component labelling to label them uniquely. A 32-bit depth was required after finding that 8-bit (i.e., 2^8 labels) and 16-bit (i.e., 2^{16} labels) images were not enough to label all the candidate vessel sections. The resulting stack is called the 'labelled' stack from here on in, where each individual candidate vessel section is labelled numerically. We only considered candidate vessel sections that appear across the whole scan depth (Figure 1g), which we call 'spanning vessel sections'. These correspond to xylem vessels for which we can be confident we can make representative measurements. To determine spanning vessel sections, we checked which labels appear on both top and bottom slices of the labelled stack. Only diameters associated with spanning vessel sections are reported in our results.

We measured diameters of the vessel sections using the *Thickness* function in the BoneJ plug-in of ImageJ (Doube et al., 2010), which

we applied to the vessel sections in the original segmented stacks (pre-3D-erosion) so the diameter measurements would not be affected by the processing required for unique labelling. The thickness function uses 3D sphere fitting to calculate the maximum thickness of the segmented vessel section at each voxel. This maintains continuity of our diameter measurements across the depth of each component, and thus makes the characterization of each diameter measurement three dimensional. The resulting stack is called the 'thickness' stack from here on in.

We used the labelled and thickness stacks together to quantify each individual vessel's diameter at every depth in the scan using Python v. 3.9 (Van Rossum & Drake, 2009). For each vessel section in the labelled stack, uniquely identified by its label, we created a mask by retaining only voxels corresponding to that vessel, setting the rest to background. By overlaying this mask with the thickness stack, we could then isolate that vessel section within the thickness stack. We then considered the maximum pixel value of the resulting stack, corresponding to the maximum diameter of the vessel, on each slice (at each $1\ \mu\text{m}$, or voxel, depth). The diameter of the vessel section was considered as the mean of these maximum diameters over all slices. This process assumes the mean diameter is representative over the considered vessel section. As such, we calculated

the mean of vessel section diameter variances within each scan, the mean square within (MSW), to check the diameters of the considered vessel sections across their depth did not deviate too far from the reported means. This is given by

$$MSW = \frac{\sum_{j=1}^n \sum_{i=1}^{1800} (d_{ij} - \bar{d}_j)^2}{((n-1) \cdot 1800)}, \quad (1)$$

where d_{ij} [m] is the maximum diameter of vessel section j on slice i , \bar{d}_j [m] is the reported mean diameter of vessel section j , 1800 is the number of image slices in the considered stacks and the number of measurements for each vessel section, and n is the number of spanning vessel sections in the scan. The denominator, $(n-1) \cdot 1800$, represents the total degrees of freedom.

2.5 | Applied statistics

All statistics were carried out using the Scipy python library (Virtanen et al., 2020). Statistics were applied on the mean representative vessel section diameter for each scan (i.e., one replicate is a scan). To determine whether statistically significant differences exist between values obtained for stems from the different cultivars, we applied a one-way analysis of variance (ANOVA). Similarly, we applied a two-tailed Student's t test to assess differences between the mean representative diameters pertaining to resistant (grouping FS17 and Leccino) versus susceptible (grouping Oglarola and Koroneiki) plants. We note that this t test accounted for the different sample sizes ($n = 5$ for susceptible, and $n = 6$ for resistant) (Virtanen et al., 2020). In addition, to assess details regarding distributions of individual vessel section diameters, we produced histograms for each cultivar corresponding to representative diameters of all vessel sections from all replicates. An ANOVA was applied to these distributions, and a two-tailed Student's t test to the corresponding distributions combining measurements from all resistant plants and from all susceptible plants. This t test could be applied by virtue of the central limit theorem. In addition, a Tukey's honestly significant difference (HSD) test was applied to the distributions to assess pairwise differences in means, and Kolmogorov–Smirnov tests were applied pairwise between the distributions to assess differences in their shapes. It should be noted that in these distribution tests, vessels within the same sample are not independent. Because of this, the statistics only test the distributions from which vessel diameters were drawn. All statistical tests were applied with a significance threshold of $p < 0.05$.

2.5.1 | Estimating susceptibility to cavitation

Vessels transport water in the plant. However, they can become embolized by air bubbles (cavitation) (Sperry & Sullivan, 1992). Xylem cavitation can occur by homogeneous nucleation, occurring when the tension

of the sap in a vessel becomes high enough that dissolved air within it expands, creating a bubble that renders the vessel no longer functional (Sperry & Tyree, 1988). However, cavitation is more likely induced by a heterogeneous nucleation, described by the 'air-seeding hypothesis' (Cochard et al., 1992; Sperry & Tyree, 1988; Tyree et al., 1994). The process of air-seeding occurs when, at critical water potential, air is pulled into water-filled vessels from adjacent, air-filled areas, such as intercellular spaces, mechanically damaged vessels or already embolized vessels. It is hypothesized that this occurs via vessel pits. As such, embolism safety is typically inferred from the pore size distribution of pit diameters (or maximum pit membrane pore diameter).

Embolism safety is inferred from pit pore sizes by invoking the Young–Laplace law. According to the Young–Laplace law, the minimum radius of an air bubble (r [m]) that can be maintained in a vessel is $r(p) = -\frac{2\gamma}{p}$, where γ [Nm⁻¹] is the surface tension at the sap–air interface, and p [Pa], the water potential (or xylem tension) (Petit et al., 2021). Thus, the largest pit pore of a vessel represents a safety barrier for embolism, as air bubbles with diameter larger than this pore will be filtered out. Importantly, there is a linear relationship between the diameter of a xylem vessel and the size of its largest pit pore (Martínez-Vilalta et al., 2002). As such, our measurements can be transformed into a scaled xylem tension at which the vessel section becomes susceptible to embolism:

$$p(r) \propto -\frac{2\gamma}{r}. \quad (2)$$

Equation 2 implies smaller air bubbles require higher tension to persist. Therefore, because larger bubbles will persist under lower tension, vessel sections with larger radii are more easily embolized than those with smaller radii. As such, we estimate the proportion of the total volume of all vessel sections (pore space) susceptible to embolism at scaled tension p , corresponding to vessel of radius r , as

$$F(p) = \frac{1}{V_{\text{tot}}} \sum_{r_i \geq r} v(r_i) \quad (3)$$

where V_{tot} [m³] is the sum of the estimated volumes of all considered vessel sections in the stem, and $v(r_i) = \pi r_i^2 \Delta z$ [m³] is the estimated volume of a vessel section of radius r_i [m] with Δz [m] stem length. In our analyses, we take $\gamma = 7.28 \times 10^{-14}$ [Pam], the surface tension at a water–air interface at 20°C.

2.5.2 | Estimating hydraulic conductivity

Healthy plant xylem passively carries water from roots to leaves via transpiration. By approximating xylem vessels as idealized cylinders, the Poiseuille relation provides an estimate of the hydraulic flow rate through a xylem vessel based on its radius (Holbrook & Zwieniecki, 2011; Zimmermann, 2013). We use this relation to infer estimates of hydraulic flow rates through the vessel sections in our stem samples based on our representative diameter measurements.

[Corrections added on 17-12-2022, after first online publication: Equations (3) and (6) have been updated in this version.]

The Poiseuille relation estimates the volumetric flow rate of sap (q [$\text{m}^3 \text{s}^{-1}$]) through an individual vessel section of radius (r_i [m]) as

$$q(r_i) = -\frac{\Delta p}{\Delta z} \frac{\pi}{8\eta} r_i^4, \quad (4)$$

where η [Pa s] is the sap viscosity and Δp [Pa] the pressure drop along the vessel section of length Δz [m]. Thus, the flow rate contributed by all vessel sections with radii less than some vessel of radius r ($Q(r)$ [$\text{m}^3 \text{s}^{-1}$]) is estimated as

$$Q(r) = \sum_{r_i \leq r} q(r_i) = \frac{\pi}{8\eta} \sum_{r_i \leq r} r_i^4 \left(-\frac{\Delta p}{\Delta z} \right). \quad (5)$$

When we consider the total flow rate contributed by all (n) vessel sections, the coefficient term in Equation 5 is considered the theoretical stem hydraulic conductivity

$$K = \frac{\pi}{8\eta} \sum_{i=1}^n r_i^4. \quad (6)$$

In our analyses, we use parameter values $\eta = 10^{-3}$ [Pa s], the viscosity of water, $\Delta z = 1.8 \times 10^{-3}$ [m] the length of the considered vessel sections, and $\Delta p = -0.1 \times 10^6$ [Pa]. We chose the value of Δp to obtain flow rates on the same order of magnitude as that implicitly measured by Dichio et al. (2013). We highlight that this analysis assumes all vessel sections are isolated and under the same water potential drop.

3 | RESULTS

3.1 | Diameter measurement characterization

We calculated the mean variance (MSW) of measurements along spanning vessel section lengths within each scan (Equation 1). The values obtained are reported in Table 1 together with the mean representative vessel section diameter. The mean variances of vessel section diameter measurements along the vessel section lengths are small relative to the mean representative diameters, suggesting the reported measurements are representative.

3.2 | Diameter measurement analysis

For each cultivar, the mean and standard deviation of mean representative vessel section diameters in each replicate (scan) is shown in Figure 2. An ANOVA showed there was no significant difference between the mean representative vessel section diameters in stems of Ogliarola, FS17 and Leccino ($p = 0.298$, $n = 3$); statistical tests between cultivars could not include Koroneiki due to only having two comparable replicates. We also considered the mean and standard deviation of mean representative vessel section diameters in all

TABLE 1 The mean of variances of all vessel section diameter measurements along their length from their representative means (MSW) (Equation 1) is given for each scan.

| Cultivar | Mean representative vessel section diameter (μm) (mean variance in diameter across vessel section lengths [μm]) for each scan |
|-----------|---|
| Koroneiki | 14.3 (1.91), 13.5 (1.92) |
| Ogliarola | 11.3 (1.39), 13.4 (1.83), 13.8 (2.15) |
| FS17 | 13.5 (1.86), 12.8 (1.57), 11.5 (2.23) |
| Leccino | 11.7 (1.87), 12.3 (1.86), 9.61 (1.25) |

resistant versus all susceptible stems (Figure 2). Although the resistant stems had on average lower mean representative vessel section diameters, a t test showed no significant difference ($p = 0.103$, $n = 5, 6$).

For each cultivar, a histogram displaying the distribution of representative vessel section diameters (across all replicates [scans]) is shown in Figure 3. An ANOVA, comparing all representative diameter measurements from all vessel sections across all scans of each cultivar (all measurements included in the distribution), showed significant differences when the cultivars were pooled. However, a Tukey's HSD showed significant differences between all pairs of cultivar vessel section diameter distribution means, except between Ogliarola and FS17. In addition, pairwise Kolmogorov-Smirnov tests showed significant differences in the shape of the distributions, except between those representing Ogliarola and FS17 (Table 2). In general, the means of all representative vessel section diameter measurements for both susceptible cultivars were larger than those for the resistant ones (Table 2). A t test comparing all representative vessel section diameter measurements from all scans of resistant and susceptible plants showed significant differences.

3.3 | Embolism susceptibility

Plant vasculature is continuously vulnerable to air embolisms, particularly under biotic and abiotic stresses. We invoked the Young-Laplace equation (Equation 2) to examine the tension at which the spanning vessel section pore space becomes susceptible to embolism given by Equation 3 (Figure 4). Statistical tests comparing the tension at which half of the pore space is susceptible to embolism found no significant differences between cultivars ($p = 0.392$, $n = 3$) or between susceptible and resistant plants ($p = 0.257$, $n = 5, 6$). The average of these tension values for each cultivar were $-19,596$ (± 379.4) Pa for Koroneiki, $-20,739$ (± 1388) Pa for Ogliarola, $-20,731$ (± 1662) Pa for FS17 and $-23,073$ (± 3318) Pa for Leccino. However, as indicated by the dashed lines (Figure 4), our results show that at the same tension at which, on average, around 40% of the pore space of Leccino stems is susceptible to embolism, around 60% of the pore space corresponding to both Ogliarola and FS17 stems are susceptible to embolism. For

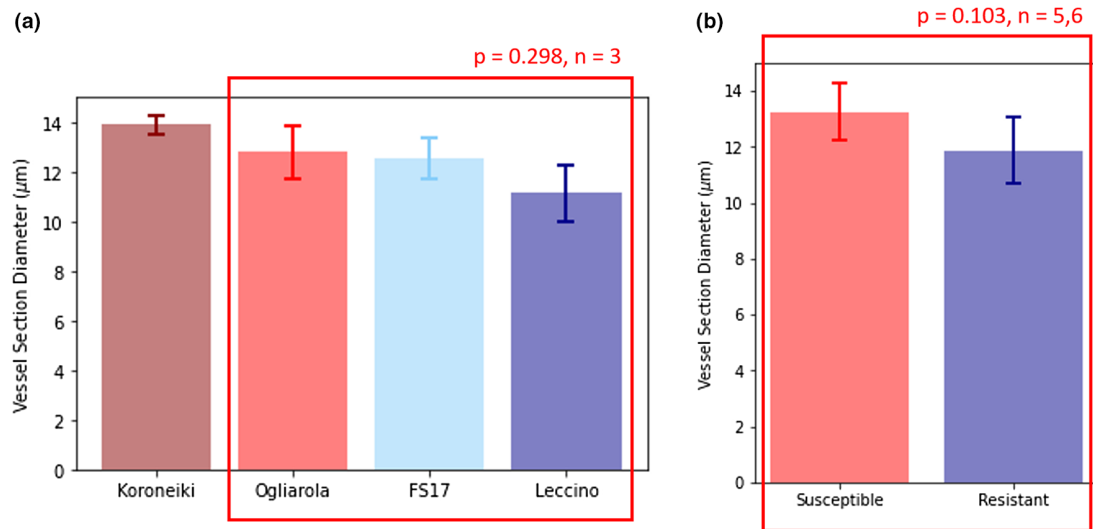


FIGURE 2 Bar plots showing the mean and standard deviation (shown by error bars) of mean vessel section diameters from replicates (scans) of different olive cultivars (a), and across all susceptible and resistant plants (b). The red boxes highlight the information used in each statistical test. These tests found no significant differences between the means of three cultivars ($p = 0.298$, $n = 3$) or between susceptible versus resistant plants ($p = 0.103$, $n = 5, 6$). [Colour figure can be viewed at [wileyonlinelibrary.com](https://onlinelibrary.wiley.com)]

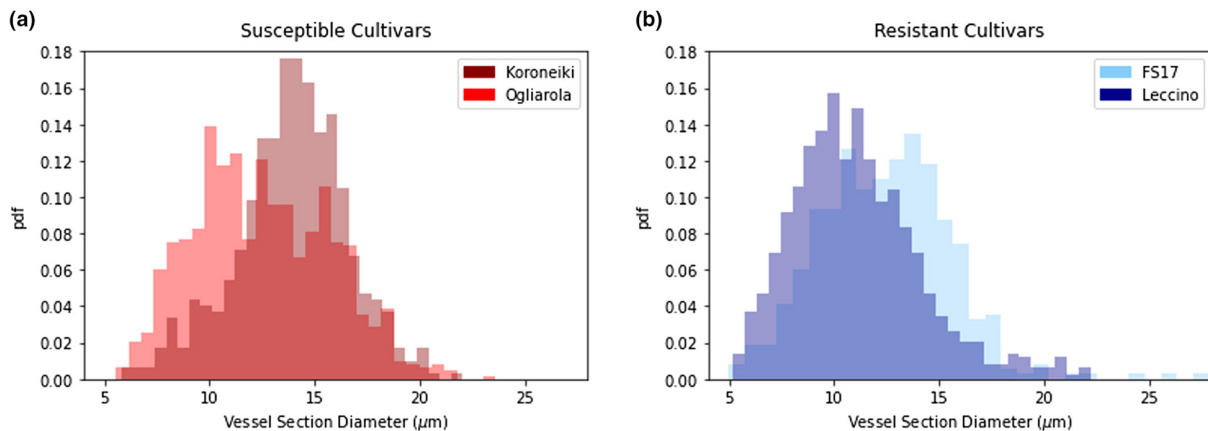


FIGURE 3 Histograms showing the probability density (pdf) distribution of vessel section diameters across all replicates (scans) for each cultivar. Histograms representing susceptible (a) and resistant (b) cultivars are shown separately. The apparent third colour in each figure represents the overlap of the presented distributions. [Colour figure can be viewed at [wileyonlinelibrary.com](https://onlinelibrary.wiley.com)]

TABLE 2 Pairwise Kolmogorov–Smirnov test outputs comparing distributions of vessel section diameter measurements between stems of different cultivars.

| | Koroneiki | Ogliarola | FS17 | Leccino |
|-----------|---------------------------------|---------------------------------|---------------------------------|---------------------------------|
| Koroneiki | $\mu = 13.93$, $\sigma = 2.64$ | $p < 0.05^*$ | $p < 0.05^*$ | $p < 0.05^*$ |
| Ogliarola | | $\mu = 12.51$, $\sigma = 3.22$ | $p = 0.105$ | $p < 0.05^*$ |
| FS17 | | | $\mu = 12.44$, $\sigma = 3.09$ | $p < 0.05^*$ |
| Leccino | | | | $\mu = 11.08$, $\sigma = 3.05$ |

Note: There are significant differences, denoted by *, between every pairing except between Ogliarola and FS17. The table diagonal shows mean and standard deviation of all diameter measurements from all vessel sections across all scans of the given cultivar; a Tukey's HSD comparing these means shows significant differences between every pairing, again except between Ogliarola and FS17.

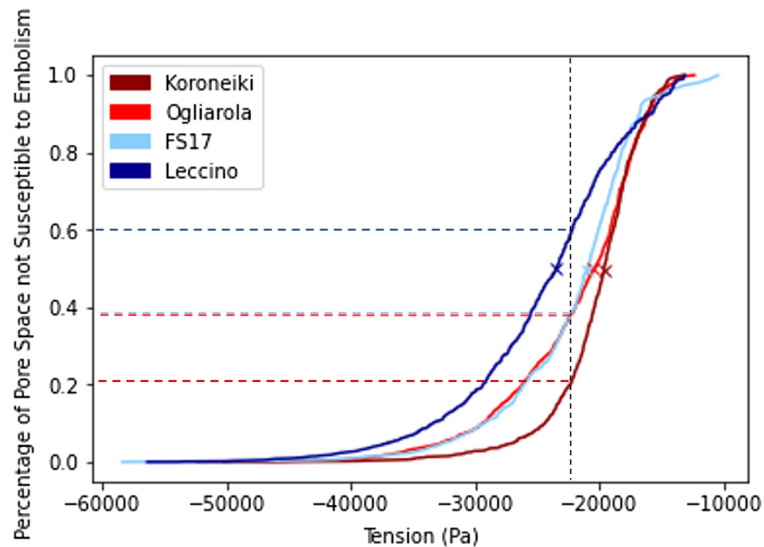


FIGURE 4 Vulnerability to embolism curves, represented by plotting tension against the percentage of pore space that certainly remains functional at the given tension determined using the Young–Laplace equation (Equation 4). We also plot (marked by x) tension values interpreted as the tension at which half the pore space is expected to be susceptible to embolism. The black dashed line indicates the tension at which on average about 40% of the pore space of Leccino stems (dark blue dashed line), about 60% of the pore space of FS17 (light blue) and Ogliarola (light red) stems, and about 80% of the pore space of Koroneiki stems (dark red) is vulnerable to embolism. [Colour figure can be viewed at wileyonlinelibrary.com]

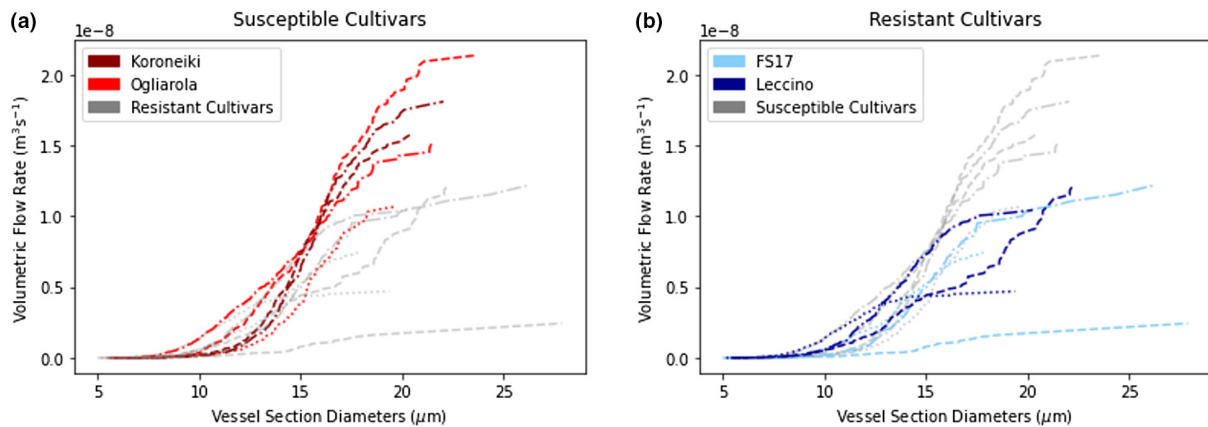


FIGURE 5 Estimate of volumetric flow rates through each scanned stem of both susceptible (a) and resistant (b) cultivars. Estimates are given by considering the cumulative contribution from vessel sections of increasing diameter. Estimates are calculated on the basis of representative vessel section diameters via the Poiseuille flow solution (Equation 6). Dashed, dotted and dash-dot lines are shown for the different replicates. On each plot we also show results for the other group of stems (in grey) to make them more easily comparable. [Colour figure can be viewed at wileyonlinelibrary.com]

Koroneiki stems, around 80% of the pore space is vulnerable at this same tension.

3.4 | Hydraulic conductivity

By approximating vessel sections as perfect cylinders, we inferred flow rates based on our diameter measurements in accordance with the Poiseuille flow solution (Equation 4). Figure 5 shows the cumulative contributions of vessel sections of increasing diameter to the volumetric flow rate (Equation 5). We then used this information to assess the impact of certain vessel section diameters being rendered nonfunctional (Figure 6), for example by air embolism. Between

contributions to flow of all considered vessel sections for each cultivar we found no significant differences ($p = 0.155$, $n = 3$) (Figure 6b). However, we did find significant differences in these measurements between resistant and susceptible plants ($p < 0.05$, $n = 5, 6$) (Figure 6c). In the previous section, we inferred that under given tension we expect the largest vessel sections to become embolized. As such we also ran the same statistical tests between contributions to flow of all considered vessel sections less than $15\ \mu\text{m}$ in diameter (Figure 6e,f), and all those less than $10\ \mu\text{m}$ in diameter (Figure 6h,i). With each removal of ‘large vessel sections’, the p values for both ANOVA and t test increased (Figure 6), suggesting that it is in fact the largest vessel sections that are responsible for much of the differences we see between cultivars in regards to hydraulic conductivity.

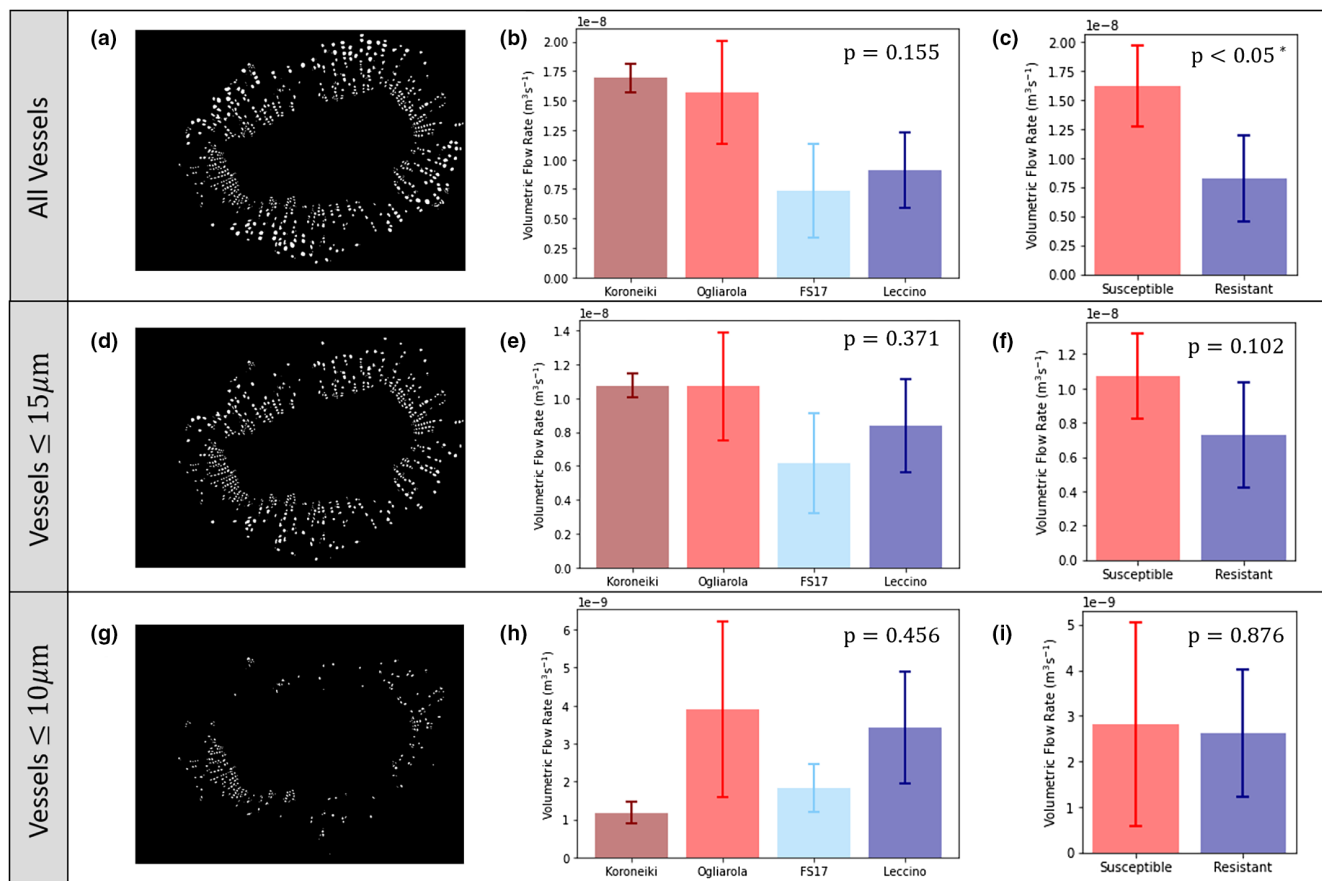


FIGURE 6 Bar plots showing the mean and standard deviation (shown by error bars) of flow rate estimates contributed by all (b, c), <math><15\ \mu\text{m}</math> (e, f) and <math><10\ \mu\text{m}</math> (h, i) diameter vessel sections across samples from different olive cultivars (b, e, h) and across all susceptible and resistant plants (c, f, i). The top slice from the scan of one replicate of Ogliarola, only showing the considered vessel sections, is given alongside the bar plots (a, d, g). Considering both an analysis of variance across cultivars and a *t* test for resistant versus susceptible plants, *p* values increased when fewer vessel sections were considered. A significant difference was obtained comparing the average flow rate through all spanning vessel sections across susceptible plants with the average across resistant plants (c). [Colour figure can be viewed at [wileyonlinelibrary.com](https://onlinelibrary.wiley.com/doi/10.1111/ppa.13674)]

4 | DISCUSSION

Current opinion suggests the use of disease-resistant plants seems the most feasible and promising long-term strategy to adapt to *X. fastidiosa* in affected regions (Chatterjee et al., 2008; Saponari et al., 2017). Despite the potential economic impact (Schneider et al., 2020), little is known about the mechanisms of resistance, and only two resistant olive cultivars have been so far identified (Baù et al., 2017; Boscia et al., 2017). One feature thought to be important to the resistance of some cultivars to *X. fastidiosa* infection is a difference in xylem vessel diameters. Several cases have been described in which plant resistance to vascular pathogens is related to narrower vessels (Chatelet et al., 2011; Elgersma, 1970; Petit et al., 2021; Pouzoulet et al., 2017; Sabella et al., 2019). Both Chatelet et al. (2011) and Deyett et al. (2019) find significantly smaller diameter vessels in *X. fastidiosa*-tolerant grape cultivar Sylvaner compared with more susceptible cultivars. The hypothesis that narrower xylem vessels are linked to disease resistance in grapevine is also evidenced in the context of the vascular wilt pathogen *Phaeoaniella chlamydospora* (Pouzoulet et al., 2017, 2019, 2020).

In the context of olives, previous studies have found vessels in *X. fastidiosa*-resistant olive cultivar Leccino to be narrower than those in susceptible cultivar Cellina di Nardò (Petit et al., 2021; Sabella et al., 2019). Some work has been done to understand how vessel diameters could influence disease susceptibility. In particular, the studies of Pouzoulet et al. (2019, 2020) provide evidence that vessel diameter directly impacts the efficiency of the compartmentalization process. It is without question that host susceptibility to vascular wilt is influenced by the ability of the pathogen to spread through the vasculature, which itself is a direct consequence of compartmentalization. We argue that, on the basis of this fundamental physical reasoning, it is highly likely that a bias towards narrower xylem vessels is relevant for resistance in a much wider variety of plant vascular pathogens and hosts. While Coletta-Filho et al. (2007) found the opposite trend among Pera sweet orange × Murcott tangor hybrids, that is, they found that *X. fastidiosa*-resistant plants had on average larger diameter xylem vessels than susceptible ones, they found no correlation with disease resistance. We anticipate that this result may be due to the fact that only the average vessel diameter is presented for each cultivar, rather than a consideration of the full-size

distributions. There is evidence that in the case of grapevine, it is an absence or limited presence of the largest diameter vessels that is correlated with cultivar resistance (Pouzoulet et al., 2020). There is some evidence that this may also be the case for olive trees (Sabella et al., 2019); however, further investigation is needed. In this study, by taking detailed vessel diameter distributions derived from 3D measurements, we were able to obtain a more complete picture of the geometry than was possible in previous studies. In addition, by considering four different olive cultivars, we could obtain more nuanced insights into the relevance of geometric trends on resistance across a range of cultivars of varying susceptibility. By applying fundamental theoretical relationships, we could also further extend the hypothesis made by previous authors by then inferring the mechanisms by which a greater proportion of narrower vessels may contribute to resistance. We test both the relevance of diameter on susceptibility to embolism, in a similar manner to Petit et al. (2021), but also additionally on hydraulic conductivity. As a further extension to the work of Petit et al. (2021), we highlight the trade-offs between these two aspects: embolism safety and maintenance of hydraulic functionality. Furthermore, we extend the utility of the Young–Laplace equation to discuss subsequent vessel susceptibility to embolism developments, which have previously been limited to pit inferences.

There was no statistically significant difference in the mean representative vessel section diameters from replicates of three cultivars, or between the mean representative vessel section diameters from resistant versus susceptible plants. However, we acknowledge that this result may be influenced by the fact that we were limited in the number of replicates due to the intensive scan time required to achieve the necessary resolution. Despite being limited by the number of replicates, we measured every segmented object within each scan to enable a robust analysis of trends in vessel section diameters. This process resulted in the quantification of about 500 dominant spanning vessel sections. Previous studies relied on measuring diameters manually and were thus limited to many fewer measurements (Sabella et al., 2019). Qualitatively, comparing resistant versus susceptible plants, our results agree with the studies of Sabella et al. (2019) and Petit et al. (2021) that compared vessel diameter measurements of cultivars Leccino and Cellina di Nardò. Comparing distributions of all spanning vessel section diameters from two susceptible and two resistant olive cultivars, we found significant differences in both the cultivar distributions (ANOVA) and in the distributions corresponding to resistant versus susceptible plants (*t* test). In addition, mean diameters of vessel sections from stems of the two resistant cultivars were smaller than those from stems of the two susceptible cultivars. However, a Tukey's HSD showed significant differences between all pairs of cultivar vessel section diameter distribution means other than between Ogliarola and FS17. In addition, our results showed significant differences comparing the shapes of the distributions (Kolmogorov–Smirnov tests), except again when we compared those corresponding to Ogliarola and FS17. This suggests differences in xylem vessel diameter distributions may play a significant role regarding the resistance of Leccino, but not the

relative susceptibility and resistance of Ogliarola and FS17. By considering more than just one susceptible and one resistant cultivar, we have highlighted that different resistance traits may have variable influence on the relative resistance of cultivars. This may explain why the mean representative vessel section diameter between resistant and susceptible stems were not significantly different. It would be naive to assume that redundancies in resistance would not exist. For example, it has been shown that two drought-tolerant wheat cultivars have different resistance mechanisms (Chu et al., 2021). There are clear parallels between vascular wilts and drought; the wilting of plants infected by vascular pathogens results directly, at least in part, from the same plant responses activated in drought conditions, namely the formation of tyloses and gels. Thus, natural parallels can also be drawn between the ways in which plants mitigate against such biotic and abiotic stresses. In particular, we note that there are a number of instances where plant traits have been related to both enhanced disease resistance and improved drought tolerance (Qiu & Yu, 2009; Shi et al., 2011; Sohn et al., 2006). It is well documented that the structure of plant vasculature is governed by a trade-off with regards to embolism safety and transpiration (Maherali et al., 2004, 2006; Meinzer et al., 2010). There is no reason to assume that different cultivars would strike the same balance between these two aspects; in particular, there are a number of instances where different degrees of drought tolerance among different cultivars has been observed. For example, two different drought-tolerant almond cultivars have been identified as having different resistance mechanisms to drought (Torrecillas et al., 1996). Both cultivars are effective at maintaining reasonable functionality during drought conditions. However, due to maintaining higher yield under deficit irrigation strategies, the authors conclude that, as a result of its particular tolerance mechanisms, one of the two cultivars is more efficient at coping with water stress than the other (Torrecillas et al., 1996). Though it is not clear why the two cultivars have not both developed the more efficient resistance mechanisms, we can speculate that some mechanisms come at certain costs that may not be or may not have yet become feasible for one cultivar due to differences in either internal or external pressures. We expect that there is likely to be an analogous variation in degree of resistance among different cultivars of species vulnerable to various vascular wilt pathogens. We anticipate that the resistance of FS17 may instead be more greatly influenced by factors not directly related to vessel geometry, which have previously only been investigated in relation to Leccino. For example, transcriptome analyses of naturally infected Leccino and Ogliarola Salentina (Giampetruzzi et al., 2016) identified a number of differentially expressed genes with those encoding receptor-like kinases and receptor-like proteins being up-regulated in Leccino (Choi et al., 2013). Some of these receptor-like molecules could function as pattern recognition receptors (Rapicavoli et al., 2018) that would activate the plant immune response. Similar genes encoding receptor-like molecules may also be up-regulated in FS17. Another study suggests that lignin may play a critical role in resistance; a significant total increase in lignin in infected Leccino in comparison to infected Cellina di Nardò, and differing lignin distribution in the

xylem of healthy versus infected Leccino plants was found (Sabella et al., 2018). These authors hypothesized that increased levels of lignin in xylem vessels of infected Leccino plants could represent pits in the vessel walls becoming less easily degradable by *X. fastidiosa* cells. This would make the bacteria less able to move into adjacent vessels, ultimately delaying disease progression. The role of lignin in the resistance of FS17 should also be investigated. Another mechanism that may be relevant to the resistance of FS17 relates to the management of the defence response. This again has already been investigated in Leccino. Authors found that Leccino had a better management of the defence response regarding the production of tyloses and gels in comparison with both Ogliarola Saletina and Cellina di Nardò (De Benedictis et al., 2017). Future studies investigating the relevance of these mechanisms to the resistance of FS17 could provide critical insights beyond the scope of this work.

We also investigated whether we could obtain insights regarding the differences in xylem vessel section diameter distributions as a source of resistance to the physical mechanisms of the plant response to disease. The mechanisms by which resistance traits keep bacterial populations low and limit disease symptoms are often overlooked in previous studies. One study found a correlation between the susceptibility of two cultivars to air embolism and their susceptibility to *X. fastidiosa* infection (Petit et al., 2021). These authors hypothesized this could be a result of differences in vessel diameters. We investigated this by theoretical means. At first glance, evaluating tensions at which 50% of the pore space is susceptible to embolism, we did not find statistically significant differences between three cultivars (ANOVA) or between resistant versus susceptible plants (*t* test). However, produced embolism vulnerability curves have more nuanced physical meaning. The curves show that, for example, at the tension at which on average about 40% of the pore space of Leccino stems is susceptible to embolism, on average, about 60% of the pore space corresponding to both Ogliarola and FS17 stems is susceptible to embolism. This is even more critical for Koroneiki stems, for which about 80% of the pore space is vulnerable at this same tension. This result highlights that small differences in tension can have drastic impacts on vessel functionality based on the detailed vessel distributions. Our results also show qualitative consistency with measurements of Petit et al. (2021). These authors found susceptible cultivar Cellina di Nardò to be more vulnerable to air embolism than resistant cultivar Leccino; a mean loss in conductance of about 58% was measured in Cellina di Nardò, in comparison to about 38% in Leccino under the same conditions. It was hypothesized by Petit et al. (2021) that this relates to *X. fastidiosa* resistance by the fact that a greater number of air embolisms would be more favourable for the aerobic metabolism of the bacteria, and, particularly in drought conditions, results in a larger proportion of the xylem becoming non-functional. As a caveat, some studies have reported that *X. fastidiosa* exhibits growth more closely resembling that of a facultative anaerobe (Shriner & Andersen, 2014). Oxidic conditions may still be beneficial for the bacteria; however, further studies are needed to explore colonies in oxygen-limited environments. It would be reasonable to hypothesize that a relatively high loss of xylem functionality due

to air embolism could exacerbate disease symptoms in susceptible cultivars. However, our inferences pertaining to estimated hydraulic flow rates suggest that even under conditions allowing the largest vessels to be embolized, the hydraulic flow rates in susceptible cultivars remain above, if not comparable to, those in resistant cultivars.

Most symptoms of *X. fastidiosa* infection are similar to those of water stress, and thus it is expected that the susceptibility of a cultivar should correlate to its ability to transpire water. We found that, on average, the considered susceptible cultivars had greater theoretical volumetric flow rates than the considered resistant cultivars. Though we did not find statistically significant differences between mean theoretical flow rates for three cultivars, we did find a statistically significant difference between those for susceptible compared with resistant plants. This result suggests that, due to having higher stem hydraulic conductivity, susceptible cultivars are able to transpire water at faster rates than resistant ones under ideal conditions. This is consistent with previous findings (Petit et al., 2021). Similarly transforming vessel diameter measurements using the Hagen Poiseuille equation (Equation 8), Petit et al. (2021) showed that comparable stems from resistant cultivar Leccino are consistently less conductive, corresponding to slower flow rates, than those from susceptible cultivar Cellina di Nardò. We hypothesize that this corresponds to the fact that, after inoculation, the faster flow rates in the xylem of susceptible cultivars could be more effective in spreading the pathogen through the plant. This is an important insight into the potential influence of xylem physiology on the early stages of infection. Our theoretical flow rates not only support the findings of Petit et al. (2021), but, in conjunction with our inferences pertaining to embolism susceptibility, also suggest a mechanism that may influence a plant's susceptibility to *X. fastidiosa* during later stages of infection. During the early colonization phase, *X. fastidiosa* bacteria do not produce adhesins or gums, but rather pit degrading enzymes (Chatterjee et al., 2008). It is understood that the enlargement of pit pores via degradation probably has serious negative consequences on water transport linked to the formation and spread of air emboli (Petit et al., 2021). If the bacteria are more mobile in the early stages of infection, there is greater opportunity for pit degradation and thus, in the later stages of infection, air embolisms. We considered the effect of removing the flow rate contribution from vessel sections with diameter $\geq 15 \mu\text{m}$ and $\geq 10 \mu\text{m}$, corresponding to a theoretical scenario in which these vessel sections are embolized or no longer functional. In doing so, *p* values comparing three cultivars and resistant versus susceptible plants increased. The importance of this becomes clear when we consider the relative effect of these large vessel sections becoming embolized in stems of the respective cultivars. In Figure 4, if the largest vessel sections are embolized, this corresponds to the loss of a greater proportion of the overall vessel pore space for susceptible plants compared with resistant plants. If the remaining non-embolized vasculature in both susceptible and resistant cultivars have similar magnitudes of hydraulic conductance, this would suggest that the susceptible cultivars support faster flow rates than the resistant cultivars with less of their total vasculature. Over longer time spans postinfection, this will result in extra stress being imposed on the

remaining non-embolized vasculature in the susceptible plant, which can lead to damage of the vasculature. In contrast, the redundancy in xylem vasculature in resistant cultivars can potentially act to redistribute these stresses, thus reducing risk to damage. We hypothesize that this stress would be significant to the relative susceptibility and resistance of different cultivars to *X. fastidiosa* infection. We suggest future studies try to capture this effect experimentally by considering hydrated stems under different pressure conditions.

X-ray CT allowed for a 3D quantification of vessel section diameters on the basis of an average of measurements obtained by sphere fitting across entire vessel section lengths. To check the diameter of a considered (spanning) vessel section across its length did not deviate too far from its reported mean, we calculated the mean variance of measurements along each vessel section within each scan (Equation 1). The values reported are relatively small, about 1–2 μm , compared to the average reported means, which are about 10–14 μm (Table 1). This gave us confidence that the mean vessel section diameter is representative. Previous studies that report vessel diameters often rely on a few 2D cross sections from spread out stem locations. X-ray CT images have the advantage over traditional thin-slicing microscopy of maintaining consistent alignment across slices. Our calculated mean vessel section diameters could be approximated using 1800 2D cross-sectional images at every 1 μm depth. However, we note that this is two orders of magnitude more images than is typical in previous studies. Additionally, in actuality, our diameters result from thickness maps that treat the image stack as a 3D data. Because of this, our measurements preserve diameter continuity of the spanning vessel sections across their length. This also meant we could ensure that we did not over-represent certain vessel sections that may appear in multiple cross sections. Lastly, we note that previous studies present measurements of vessels that are selected without any explicitly specified method. By considering just the spanning vessel sections, which we assume are dominant in conducting water, we present a consistent selection method that takes into account xylem functionality.

In conclusion, we show differences in the distributions of vessel section diameters from stems of olive cultivars of varying susceptibility to *X. fastidiosa*. Importantly, we find it is the relative dominance of larger vessels to the pore space of susceptible cultivars that has a significant influence on xylem hydraulic conductivity and vulnerability to air embolism, which we hypothesize to be relevant for disease dynamics. As a result of this, a xylem morphological screening may be useful to identify some resistant cultivars. However, because we did not find differences in the diameter distributions of vessel sections from stems of Ogliarola compared with FS17, we suggest a more successful screening protocol would probably include multiple stages of which xylem morphology would constitute only one stage. As such, we propose future work should assess differences in other factors that could be efficiently tested across an appropriate range of cultivars and a large number of replicates.

Furthermore, extension of current modelling protocols can aid to better identify the causes for symptoms. Future studies can expand on the current flow considerations to explicitly consider

biofilm development within the host, estimate bacterial spreading through fluid transport and even consider plant responses to try and mitigate plant dieback. Lastly, 3D images can provide further insights into *X. fastidiosa* transport within a host considering exact vessel geometries by image-based modelling. These in silico experiments will be able to provide further hypotheses for screening protocols.

ACKNOWLEDGEMENTS

N.C.W. and T.R. are funded by NERC grant NE/S00720/1. S.M.W. is funded by the European Union's Horizon 2020 Research and Innovation Programme under grant agreement number 727987-XF-ACTORS 'Xylella Fastidiosa Active Containment Through a Multidisciplinary-Oriented Research Strategy', the grant agreement number 734353-CURE-XF 'Capacity Building and Raising Awareness in Europe and in Third Countries to Cope with Xylella fastidiosa' and by the BRIGIT project by UK Research and Innovation through the Strategic Priorities Fund, by a grant from Biotechnology and Biological Sciences Research Council, with support from the Department for Environment, Food and Rural Affairs and the Scottish Government (BB/S016325/1). K.A.W., S.A.R., C.P., D.M.F. and T.R. are funded by ERC Consolidator grant 646809 (Data Intensive Modelling of the Rhizosphere Processes). M.S. and A.D.S. are funded by the European Union's Horizon 2020 Research and Innovation Programme under grant agreement number 635646-PONTE 'Pest Organisms Threatening Europe' and the grant agreement number 727987-XF-ACTORS 'Xylella fastidiosa Active Containment Through a Multidisciplinary-Oriented Research Strategy'. T.R. is also funded by BBSRC SARIC BB/P004180/1, BBSRC SARISABB/L025620/1 and EPSRC EP/M020355/1. The authors acknowledge the μ -VIS X-ray Imaging Centre at the University of Southampton for the provision of the X-ray tomographic imaging facilities.

DATA AVAILABILITY STATEMENT

All data supporting this study are available from the University of Southampton repository on request at <https://doi.org/10.5258/SOTON/D2209>.

ORCID

Steven M. White  <https://orcid.org/0000-0002-3192-9969>

Kathryn E. Rankin  <https://orcid.org/0000-0002-8458-1038>

Tiina Roose  <https://orcid.org/0000-0001-8710-1063>

REFERENCES

- Agrios, G.N. (2005) *Plant pathology*. Amsterdam: Elsevier.
- Baù, A., Delbianco, A., Stancanelli, G. & Tramontini, S. (2017) Susceptibility of *Olea europaea* L. varieties to *Xylella fastidiosa* subsp. *pauca* ST53: systematic literature search up to 24 March 2017. *EFSA Journal*, 15, e04772.
- Boscia, D., Altamura, G., Ciniero, A., Di Carolo, M., Dongiovanni, C., Fumarola, G. et al. (2017) Resistenza a *Xylella fastidiosa* in diverse cultivar di olivo. *L'Informatore Agrario*, 11, 59–63.
- Bragard, C., Dehnen-Schmutz, K., Di Serio, F., Gonthier, P., Jacques, M.A., Miret, J.A.J. et al. (2019) Effectiveness of in planta control measures for *Xylella fastidiosa*. *EFSA Journal*, 17, e05666.

- Cardinale, M., Luvisi, A., Meyer, J.B., Sabella, E., De Bellis, L., Cruz, A.C. et al. (2018) Specific fluorescence in situ hybridization (FISH) test to highlight colonization of xylem vessels by *Xylella fastidiosa* in naturally infected olive trees (*Olea europaea* L.). *Frontiers in Plant Science*, 9, 431.
- Chatelet, D.S., Wistrom, C.M., Purcell, A.H., Rost, T.L. & Matthews, M.A. (2011) Xylem structure of four grape varieties and 12 alternative hosts to the xylem-limited bacterium *Xylella fastidiosa*. *Annals of Botany*, 108, 73–85.
- Chatterjee, S., Almeida, R.P.P. & Lindow, S. (2008) Living in two worlds: the plant and insect lifestyles of *Xylella fastidiosa*. *Annual Review of Phytopathology*, 46, 243–271.
- Choi, H.-K., Iandolino, A., Da Silva, F.G. & Cook, D.R. (2013) Water deficit modulates the response of *Vitis vinifera* to the Pierce's disease pathogen *Xylella fastidiosa*. *Molecular Plant-Microbe Interactions*, 26, 643–657.
- Chu, C., Wang, S., Paetzold, L., Wang, Z., Hui, K., Rudd, J.C. et al. (2021) RNA-seq analysis reveals different drought tolerance mechanisms in two broadly adapted wheat cultivars 'TAM 111' and 'TAM 112'. *Scientific Reports*, 11, 4301.
- Cochard, H., Cruziat, P. & Tyree, M.T. (1992) Use of positive pressures to establish vulnerability curves: further support for the air-seeding hypothesis and implications for pressure-volume analysis. *Plant Physiology*, 100, 205–209.
- Coletta-Filho, H., Pereira, E., Souza, A., Takita, M., Cristofani-Yale, M. & Machado, M. (2007) Analysis of resistance to *Xylella fastidiosa* within a hybrid population of Pera sweet orange × Murcott tangor. *Plant Pathology*, 56, 661–668.
- Collins, B.R., Parke, J.L., Lachenbruch, B. & Hansen, E.M. (2009) The effects of *Phytophthora ramorum* infection on hydraulic conductivity and tylosis formation in tanoak sapwood. *Canadian Journal of Forest Research*, 39, 1766–1776.
- D'Attoma, G., Morelli, M., Saldarelli, P., Saponari, M., Giampetruzzi, A., Boscia, D. et al. (2019) Ionomeric differences between susceptible and resistant olive cultivars infected by *Xylella fastidiosa* in the outbreak area of Salento, Italy. *Pathogens*, 8, 272.
- De Benedictis, M., De Caroli, M., Baccelli, I., Marchi, G., Blevé, G., Gallo, A. et al. (2017) Vessel occlusion in three cultivars of *Olea europaea* naturally exposed to *Xylella fastidiosa* in open field. *Journal of Phytopathology*, 165, 589–594.
- De Micco, V., Balzano, A., Wheeler, E.A. & Baas, P. (2016) Tyloses and gums: a review of structure, function and occurrence of vessel occlusions. *IAWA Journal*, 37, 186–205.
- De Pascali, M., Vergine, M., Negro, C., Greco, D., Vita, F., Sabella, E. et al. (2022) *Xylella fastidiosa* and drought stress in olive trees: a complex relationship mediated by soluble sugars. *Biology*, 11, 112.
- De Pascali, M., Vergine, M., Sabella, E., Aprile, A., Nutricati, E., Nicoli, F. et al. (2019) Molecular effects of *Xylella fastidiosa* and drought combined stress in olive trees. *Plants*, 8, 437.
- Delbianco, A., Gibin, D., Pasinato, L. & Morelli, M. (2022) Update of the *Xylella* spp. host plant database – systematic literature search up to 30 June 2021. *EFSA Journal*, 20, e07039.
- Deyett, E., Pouzoulet, J., Yang, J.I., Ashworth, V.E., Castro, C., Roper, M.C. et al. (2019) Assessment of Pierce's disease susceptibility in *Vitis vinifera* cultivars with different pedigrees. *Plant Pathology*, 68, 1079–1087.
- Dichio, B., Montanaro, G., Sofo, A. & Xiloyannis, C. (2013) Stem and whole-plant hydraulics in olive (*Olea europaea*) and kiwifruit (*Actinidia deliciosa*). *Trees*, 27, 183–191.
- D'Onghia, A.M., Santoro, F., Gualano, S., Valentini, F., Minutillo, S., Frasher, D. et al. (2021) Specific sampling schemes for effective surveillance program. Available at: <https://cordis.europa.eu/project/id/727987/results> [Accessed 1 November 2022]
- Doube, M., Kłosowski, M.M., Arganda-Carreras, I., Cordelières, F.P., Dougherty, R.P., Jackson, J.S. et al. (2010) BoneJ: free and extensible bone image analysis in ImageJ. *Bone*, 47, 1076–1079.
- Elgersma, D.M. (1970) Length and diameter of xylem vessels as factors in resistance of elms to *Ceratocystis ulmi*. *Netherlands Journal of Plant Pathology*, 76, 179–182.
- European Union. (2017) Commission implementing decision (EU) 2017/2352 amending implementing decision 2015/789 as regards measures to prevent the introduction into and the spread within the union of *Xylella fastidiosa* (Wells et al.). Official Journal of the European Union L 336/31.
- Giampetruzzi, A., Baptista, P., Morelli, M., Cameirão, C., Neto, T.L., Costa, D. et al. (2020) Differences in the endophytic microbiome of olive cultivars infected by *Xylella fastidiosa* across seasons. *Pathogens*, 9, 723.
- Giampetruzzi, A., Morelli, M., Saponari, M., Loconsole, G., Chiumenti, M., Boscia, D. et al. (2016) Transcriptome profiling of two olive cultivars in response to infection by the CoDiRO strain of *Xylella fastidiosa* subsp. *pauca*. *BMC Genomics*, 17, 475.
- Holbrook, N.M. & Zwieniecki, M.A. (2011) *Vascular transport in plants*. Amsterdam: Elsevier.
- Krivanek, A. & Walker, M. (2005) *Vitis* resistance to Pierce's disease is characterized by differential *Xylella fastidiosa* populations in stems and leaves. *Phytopathology*, 95, 44–52.
- Landis, E.N. & Keane, D.T. (2010) X-ray microtomography. *Materials Characterization*, 61, 1305–1316.
- Luvisi, A., Aprile, A., Sabella, E., Vergine, M., Nicoli, F., Nutricati, E. et al. (2017) *Xylella fastidiosa* subsp. *pauca* (CoDiRO strain) infection in four olive (*Olea europaea* L.) cultivars: profile of phenolic compounds in leaves and progression of leaf scorch symptoms. *Phytopathologia Mediterranea*, 56, 259–273.
- Maherali, H., Moura, C.F., Caldeira, M.C., Willson, C.J. & Jackson, R.B. (2006) Functional coordination between leaf gas exchange and vulnerability to xylem cavitation in temperate forest trees. *Plant, Cell & Environment*, 29, 571–583.
- Maherali, H., Pockman, W.T. & Jackson, R.B. (2004) Adaptive variation in the vulnerability of woody plants to xylem cavitation. *Ecology*, 85, 2184–2199.
- Martínez-Vilalta, J., Prat, E., Oliveras, I. & Piñol, J. (2002) Xylem hydraulic properties of roots and stems of nine Mediterranean woody species. *Oecologia*, 133, 19–29.
- McElrone, A.J., Grant, J.A. & Kluepfel, D.A. (2010) The role of tyloses in crown hydraulic failure of mature walnut trees afflicted by apex disorder. *Tree Physiology*, 30, 761–772.
- Meinzer, F.C., McCulloh, K.A., Lachenbruch, B., Woodruff, D.R. & Johnson, D.M. (2010) The blind men and the elephant: the impact of context and scale in evaluating conflicts between plant hydraulic safety and efficiency. *Oecologia*, 164, 287–296.
- Montilon, V., De Stradis, A., Saponari, M., Kubaa, R.A., Giampetruzzi, A., D'Attoma, G. et al. (2022) *Xylella fastidiosa* subsp. *pauca* ST53 exploits pit membranes of susceptible olive cultivars to spread systematically in the xylem. *Plant Pathology*. Available from: <https://doi.org/10.1111/ppa.13646>
- Muzzalupo, I., Stefanizzi, F. & Perri, E. (2009) Evaluation of olives cultivated in southern Italy by simple sequence repeat markers. *HortScience*, 44, 582–588.
- Ollion, J., Cochennec, J., Loll, F., Escudé, C. & Boudier, T. (2013) TANGO: a generic tool for high-throughput 3D image analysis for studying nuclear organization. *Bioinformatics*, 29, 1840–1841.
- Otsu, N. (1979) A threshold selection method from gray-level histograms. *IEEE Transactions on Systems, Man, and Cybernetics*, 9, 62–66.
- Pavan, S., Vergine, M., Nicoli, F., Sabella, E., Aprile, A., Negro, C. et al. (2021) Screening of olive biodiversity defines genotypes potentially resistant to *Xylella fastidiosa*. *Frontiers in Plant Science*, 12, 723879.
- Petit, G., Blevé, G., Gallo, A., Mita, G., Montanaro, G., Nuzzo, V. et al. (2021) Susceptibility to *Xylella fastidiosa* and functional xylem anatomy in *Olea europaea*: revisiting a tale of plant-pathogen interaction. *AoB Plants*, 13, plab027.

- Pouzoulet, J., Rolshausen, P.E., Charbois, R., Chen, J., Guillaumie, S., Ollat, N. et al. (2020) Behind the curtain of the compartmentalization process: exploring how xylem vessel diameter impacts vascular pathogen resistance. *Plant, Cell & Environment*, 43, 2782–2796.
- Pouzoulet, J., Scudiero, E., Schiavon, M. & Rolshausen, P.E. (2017) Xylem vessel diameter affects the compartmentalization of the vascular pathogen *Phaeoemoniella chlamydospora* in grapevine. *Frontiers in Plant Science*, 8, 1442.
- Pouzoulet, J., Scudiero, E., Schiavon, M., Santiago, L.S. & Rolshausen, P.E. (2019) Modeling of xylem vessel occlusion in grapevine. *Tree Physiology*, 39, 1438–1445.
- Qiu, Y. & Yu, D. (2009) Over-expression of the stress-induced *OsWRKY45* enhances disease resistance and drought tolerance in *Arabidopsis*. *Environmental and Experimental Botany*, 65, 35–47.
- Rapicavoli, J., Ingel, B., Blanco-Ulate, B., Cantu, D. & Roper, C. (2018) *Xylella fastidiosa*: an examination of a re-emerging plant pathogen. *Molecular Plant Pathology*, 19, 786–800.
- Roper, C., Castro, C. & Ingel, B. (2019) *Xylella fastidiosa*: bacterial parasitism with hallmarks of commensalism. *Current Opinion in Plant Biology*, 50, 140–147.
- Rueden, C.T., Schindelin, J., Hiner, M.C., DeZonia, B.E., Walter, A.E., Arena, E.T. et al. (2017) ImageJ2: ImageJ for the next generation of scientific image data. *BMC Bioinformatics*, 18, 529.
- Sabella, E., Aprile, A., Genga, A., Siciliano, T., Nutricati, E., Nicoli, F. et al. (2019) Xylem cavitation susceptibility and refilling mechanisms in olive trees infected by *Xylella fastidiosa*. *Scientific Reports*, 9, 9602.
- Sabella, E., Luvisi, A., Aprile, A., Negro, C., Vergine, M., Nicoli, F. et al. (2018) *Xylella fastidiosa* induces differential expression of lignification related-genes and lignin accumulation in tolerant olive trees cv. Leccino. *Journal of Plant Physiology*, 220, 60–68.
- Saponari, M., Altamura, G., Abou Kubaa, R., Montilon, V., Saldarelli, P., Specchia, F. et al. (2019) Further acquisition on the response of a large number of olive cultivars to infections caused by *Xylella fastidiosa* subsp. *pauca*, ST53. In: *Proceedings of the 2nd European conference on Xylella fastidiosa (how research can support solutions)*, Ajaccio, France, 2019. Available from: <https://doi.org/10.5281/zenodo.3564486>
- Saponari, M., Boscia, D., Altamura, G., Loconsole, G., Zicca, S., D'Attoma, G. et al. (2017) Isolation and pathogenicity of *Xylella fastidiosa* associated to the olive quick decline syndrome in southern Italy. *Scientific Reports*, 7, 17723.
- Saponari, M., Boscia, D., Nigro, F. & Martelli, G.P. (2013) Identification of DNA sequences related to *Xylella fastidiosa* in oleander, almond and olive trees exhibiting leaf scorch symptoms in Apulia (southern Italy). *Journal of Plant Pathology*, 95, 668.
- Saponari, M., Giampetruzzi, A., Loconsole, G., Boscia, D. & Saldarelli, P. (2019) *Xylella fastidiosa* in olive in Apulia: where we stand. *Phytopathology*, 109, 175–186.
- Schindelin, J., Arganda-Carreras, I., Frise, E., Kaynig, V., Longair, M., Pietzsch, T. et al. (2012) Fiji: an open-source platform for biological-image analysis. *Nature Methods*, 9, 676–682.
- Schneider, K., van der Werf, W., Cendoya, M., Mourits, M., Navas-Cortés, J.A., Vicent, A. et al. (2020) Impact of *Xylella fastidiosa* subspecies *pauca* in European olives. *Proceedings of the National Academy of Sciences of the United States of America*, 117, 9250–9259.
- Shi, J., Zhang, L., An, H., Wu, C. & Guo, X. (2011) GhMPK16, a novel stress-responsive group D MAPK gene from cotton, is involved in disease resistance and drought sensitivity. *BMC Molecular Biology*, 12, 22.
- Shriner, A.D. & Andersen, P.C. (2014) Effect of oxygen on the growth and biofilm formation of *Xylella fastidiosa* in liquid media. *Current Microbiology*, 69, 866–873.
- Sohn, K.H., Lee, S.C., Jung, H.W., Hong, J.K. & Hwang, B.K. (2006) Expression and functional roles of the pepper pathogen-induced transcription factor RAV1 in bacterial disease resistance, and drought and salt stress tolerance. *Plant Molecular Biology*, 61, 897–915.
- Sperry, J.S. & Sullivan, J.E. (1992) Xylem embolism in response to freeze-thaw cycles and water stress in ring-porous, diffuse-porous, and conifer species. *Plant Physiology*, 100, 605–613.
- Sperry, J.S. & Tyree, M.T. (1988) Mechanism of water stress-induced xylem embolism. *Plant Physiology*, 88, 581–587.
- Sun, Q., Sun, Y., Walker, M.A. & Labavitch, J.M. (2013) Vascular occlusions in grapevines with Pierce's disease make disease symptom development worse. *Plant Physiology*, 161, 1529–1541.
- Torrecillas, A., Alarcón, J., Domingo, R., Planes, J. & Sánchez-Blanco, M. (1996) Strategies for drought resistance in leaves of two almond cultivars. *Plant Science*, 118, 135–143.
- Tyree, M.T., Davis, S.D. & Cochard, H. (1994) Biophysical perspectives of xylem evolution: is there a tradeoff of hydraulic efficiency for vulnerability to dysfunction? *IAWA Journal*, 15, 335–360.
- Van den Bulcke, J., Boone, M., Van Acker, J., Stevens, M. & Van Hoorbeke, L. (2009) X-ray tomography as a tool for detailed anatomical analysis. *Annals of Forest Science*, 66, 1–12.
- Van Rossum, G. & Drake, F. (2009) *Python 3 reference manual*. Scotts Valley, CA: Createspace.
- Vert, M., Doi, Y., Hellwich, K.-H., Hess, M., Hodge, P., Kubisa, P. et al. (2012) Terminology for biorelated polymers and applications (IUPAC recommendations 2012). *Pure and Applied Chemistry*, 84, 377–410.
- Virtanen, P., Gommers, R., Oliphant, T.E., Haberland, M., Reddy, T., Cournapeau, D. et al. (2020) SciPy 1.0: fundamental algorithms for scientific computing in python. *Nature Methods*, 17, 261–272.
- Wells, J.M., Raju, B.C., Hung, H.-Y., Weisburg, W.G., Mandelco-Paul, L. & Brenner, D.J. (1987) *Xylella fastidiosa* gen. nov., sp. nov.: gram-negative, xylem-limited, fastidious plant bacteria related to *Xanthomonas* spp. *International Journal of Systematic and Evolutionary Microbiology*, 37, 136–143.
- Zimmermann, M.H. (2013) *Xylem structure and the ascent of sap*. Berlin: Springer Science & Business Media.

SUPPORTING INFORMATION

Additional supporting information can be found online in the Supporting Information section at the end of this article.

How to cite this article: Walker, N.C., White, S.M., Fletcher, D.M., Ruiz, S.A., Rankin, K.E. & De Stradis, A. et al. (2023)

The impact of xylem geometry on olive cultivar resistance to *Xylella fastidiosa*: An image-based study. *Plant Pathology*, 72, 521–535. Available from: <https://doi.org/10.1111/ppa.13674>